Environmental Science & Technology

Article

pubs.acs.org/est

Colorimetric Detection of Catalytic Reactivity of Nanoparticles in Complex Matrices

Charlie Corredor,[†] Mark D. Borysiak,[†] Jay Wolfer,[‡] Paul Westerhoff,[§] and Jonathan D. Posner*[,†,‡]

[†]Department of Chemical Engineering, University of Washington, Seattle, Washington 98195, United States

[‡]Department of Mechanical Engineering, University of Washington, Seattle, Washington 98195, United States

[§]School of Sustainable Engineering and the Built Environment, Arizona State University, Tempe, Arizona 85287, United States

Supporting Information

ABSTRACT: There is a need for new methodologies to quickly assess the presence and reactivity of nanoparticles (NPs) in commercial, environmental, and biological samples since current detection techniques require expensive and complex analytical instrumentation. Here, we investigate a simple and portable colorimetric detection assay that assesses the surface reactivity of NPs, which can be used to detect the presence of NPs, in complex matrices (e.g., environmental waters, serum, urine, and in dissolved organic matter) at as low as part per billion (ppb) or ng/mL concentration levels. Surface redox reactivity is a key emerging property related to potential toxicity of NPs with living cells, and is used in our assays as a key surrogate for the presence of NPs and a first tier analytical strategy toward assessing NP exposures. We detect a wide range of metal (e.g., Ag and Au) and oxide (e.g., CeO_2, SiO_2, VO_2) NPs with a diameter range of 5 to 400 nm and multiple capping agents (tannic acid (TA), polyvinylpyrrolidone (PVP), branched polyethylenimine (BPEI), polyethylene glycol (PEG)). This method is sufficiently sensitive (ppb levels) to measure concentrations typically used in toxicological studies, and uses inexpensive, commercially available reagents.

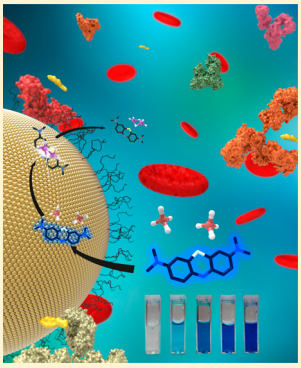

INTRODUCTION

During the past two decades, the development of nanoparticles (NPs) have rapidly increased due to their application in medicine, cosmetics, energy, manufacturing, catalysis, food preservation, etc.[1−4] Due to the widespread use of NPs, it is anticipated that nanoparticles will come into contact with humans and other biological systems.[2,5] There is a concern about the growing use of NPs in manufacturing facilities (i.e., the workplace) and consumer products that may result in adverse health and environmental impacts.[6−8] Studies have reported that nanosized particles (but not their macro or micro counterparts) can accumulate in cells and aquatic organisms that can lead to stress and mortality.[9−16] These results highlight the need for caution during the use and disposal of such manufactured nanomaterials to prevent unintended health and environmental impacts. The limitations in our current knowledge about the environmental fate and transport of NPs are partly due to the lack of simple and affordable methodology for their detection and characterization in complex samples (e.g., waste waters, lakes, oceans, foods, biological fluids, and tissues). Nanoparticles, when released to the environment and exposed to biological medium, undergo physical and chemical transformations which further complicate detection, characterization, and risk assessment.[17−19] Analytical techniques to characterize NPs include microscopy, chromatography, centrifugation, mass or light spectroscopy, electrophoretic mobility measurements, and thermo analysis.[5,20−23] However, many of these current analytical methods require highly trained personnel to operate, expensive instrumentation, and require time-consuming sample preparation and fixation that may disturb the state of particles as they existed in the environmental and biological samples. Furthermore, existing techniques usually measure mass concentrations and/or sizes, rather than the unique properties (e.g., catalytic, optical, surface plasmon resonance, surface area) of NPs that are often desired and engineered into products, and which regulators or scientist believe might cause adverse health or environmental responses. Unlike dissolved inorganic and organic chemicals where a wide spectrum of analytical techniques already exist (e.g., colorimetric detection assays to mass spectroscopy), few tiered analytical strategies are established for NPs. Here we investigate a simple colorimetric technique to detect the catalytic activity of nanoparticles, which could be used in similar ways as current colorimetric methodologies for molecular compounds (e.g., screening assays, high throughput testing, quality control, etc.) to screen for NP presence/absence in complex environmental and biological fluids.

In this paper, we report a colorimetric assay that can be used to screen for NP catalytic surface activity in biological and environmental relevant samples. Surface reactivity of nanoparticles is a key emerging property related to potential toxicity of materials with living organisms. We leverage the surface catalytic redox properties of NPs to provide a simple

Received: September 4, 2014
Revised: January 27, 2015
Accepted: January 30, 2015
Published: January 30, 2015

ACS Publications © 2015 American Chemical Society

DOI: 10.1021/es504350j
Environ. Sci. Technol. 2015, 49, 3611−3618

colorimetric detection assay. Potential applications of the catalytic assay are (i) monitoring known nanoparticles in complex media over time during lab or field studies, (ii) industrial hygiene settings where known nanoparticles are being used, and (iii) screening for the presence of unknown surface reactive nanomaterials that would be complimented later by more advanced analytical techniques for identification. Figure 1A shows a schematic representation of the catalytic electron transfer mechanism between an organic dye, methylene blue (MB), and a reducing agent, sodium borohydride (BH_4), in the presence of NP. When NPs are introduced to MB-BH_4 solution, nanoparticles serve as a catalyst for reducing the dye-reductant agent pair by promoting the electron transfer between the dye and reductant. Multiple studies report the mechanism on how nanoscale metals (but not their bulk counterparts) are catalytically active due to the reduction of their redox potential.[24,25] The literature suggests that the redox potential of NPs needs to be found between the redox potential of MB and BH_4 for it to act as a catalyst, since these reduction reactions are thermodynamically, but not kinetically, favorable.[26−29] In this case, nanoparticles serve as an electron relay in the redox reaction to transfer the electron from the donor (BH_4) to the acceptor (MB).[30,31] Reducing the dye from its oxidized state to its reduced state results in a color change from blue (oxidized state) to colorless (reduced state) due to a change in absorbance properties between the oxidized and reduced dye molecules. We plan to employ the unique surface catalytic properties of NPs as a detection approach, demonstrating its validity across a range of NPs compositions, surface coatings, and environmental/biological relevant fluids. The assay only requires a reducing agent and an organic dye for detection. Addition of NPs to the dye-reductant solution (or addition of dye-reducing agent to a suspension containing NPs) results in a rapid color change that can be inspected visually or a by portable UV−vis for improved detection capabilities. We show that the assay functions in a wide range of complex matrices and does not require elaborate sample preparation, advanced instrumentation or highly trained personnel.

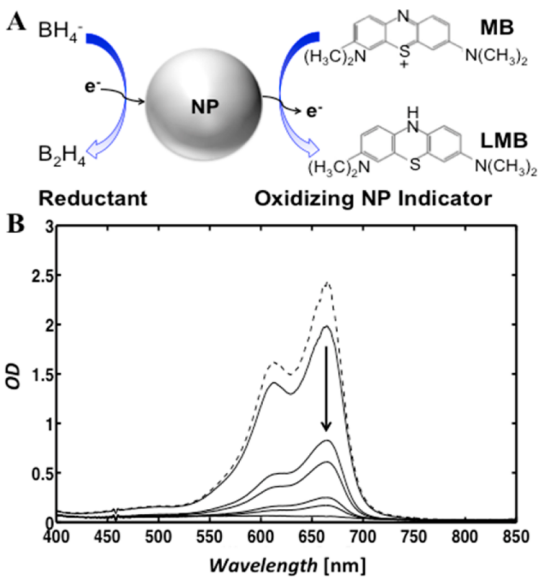

Figure 1. Schematic diagram of dye reduction electron transfer mechanism in the presence of NPs (A). Methylene blue (40 μM) and sodium borohydrate (10 mM) absorbance spectra, at 20 s time intervals, in the presence of 5 nm gold nanoparticles coated with tannic acid (Au_{TA}) at a fixed mass concentration of 1 ppm (B). Dashed lines represents initial time of NP exposure and arrow denotes the increasing time.

We have selected a dye-reductant system that (i) can be detected colorimetrically (dye has different colors in its oxidized and reduced forms); (ii) consists of a dye whose reduction is thermodynamically, but not kinetically, favorable; (iii) exhibits minimal human toxic effects, materials are not flammable, and stable at room temperature;[32] and (iv) is inexpensive for future potential use as a commercially available screening assay for NPs. We perform several experimental studies to detect commercially available NPs with a variety of core compositions (Au, Ag, CeO_2, SiO_2, and VO_2), surface coatings (tannic acid (TA), polyvinylpyrrolidone (PVP), branched polyethylenimine (BPEI), polyethylene glycol (PEG)), and sizes (5−400 nm). We use CeO_2, SiO_2, and VO_2 particles because of their large volume use in applications such as chemical mechanical planarization in the semiconductor industry,[33] energy storage,[34] catalysis,[35] and biomedicine.[36] We primarily use Au and Ag particles because of their commercial availability in a wide range of sizes and surface functionalities. Silver nanoparticles are also commonly used as a disinfectant in commercial products.[37,38] We examine the effect of NPs' concentration, size, surface area, and capping agents for this colorimetric assay in pH-buffered ultrapure water as well as in a variety of environmental and biological matrices (e.g., environmental waters, serum, urine, and dissolved organic matter). The limit of detection (LOD) and limit of quantification (LOQ) are quantified at as low as part per billion (ppb) or ng/mL.

■ EXPERIMENTAL SECTION

Environmental and Biological Matrices. In order to assess the capabilities of our dye-reductant assay to detect the presence of NPs in complex matrices, we used natural organic matter and lake water as environmental samples, serum and urine as biological matrices. An aqueous solution of 8 mg NOM/L Standard Suwannee River (SR-NOM) (International Humic Substances Society CAS: 1R101N, IHSS, MN) was prepared by dissolving SR-NOM in ultrapure water. After the solution had been prepared, it was continuously shaken and placed in a horizontal, temperature-controlled (25 °C) water-bath sonicator (Branson), where it was allowed to equilibrate for ∼24 h in the dark. This solution was subsequently calibrated for NOM concentration against UV−vis absorbance at 254 nm. Calibration experiments showed that absorbance at 254 nm was directly proportional to NOM concentration (data are not shown here). Characterization details (e.g., average molecular weight and composition) of NOM are given elsewhere.[39]

Natural waters samples were collected in polycarbonate vials from Lake Union (Seattle, WA) in May 2013 and maintained at room temperature. Before every experiment, natural water sample was continuously mixed on a rotary shaker (50 rpm) for 1 h. We used synthetic urine, prepared as described previously,[40] and serum from male and female adult mice. Our serum collection process is described in detail in the Supporting Information (SI).

Nanoparticles. We use Au nanoparticles (5, 10, 20, 50, and 100 nm nominal diameter) coated with tannic acid (TA), 20 nm Ag coated with TA, and 20 nm Au coated with polyvinylpyrrolidone (PVP), branched polyethylenimine (BPEI), polyethylene glycol (PEG). Au and Ag NPs were purchased form nanoCompsix (San Diego, CA). 150 nm CeO_2

DOI: 10.1021/es504350j
Environ. Sci. Technol. 2015, 49, 3611−3618

(CAS: CE-6082) and 20 nm SiO_2 NPs (CAS: ST-20L) were obtained from AlfaAesar (MA) and Nissan Chemical (TX), respectively. VO_2 nanoparticles were prepared utilizing the solvothermal method adopted from previous work.[41] NP concentrations presented in this study are based on manufacture reported values. In addition, we measured the total metal concentrations of NPs via ICPMS (SI Table S1). All NPs were characterized via dynamic light scattering (DLS) using a Malvern Zetasizer Nano-ZS, Westborough, MA. We measured the zeta potential and hydrodynamic diameter of NPs in the same buffering agent used in experiments (i.e., 10 mM HEPES at pH 7.0), ultra pure water, and complex matrices every 5 min for a total time of 30 min period. Hydrodynamic sizes and zeta potentials of particles are reported herein as means of triplicate measurements. Measured hydrodynamic sizes are marginally larger than the size reported by the manufacturer (SI Table S2−3). Hydrodynamic size and surface charge measurements indicate that NPs' sizes and surface charges remained relatively constant in HEPES buffer during ∼30 min period.

Experimental Methods and Materials. Nanoparticle detection studies were performed in 3 mL, disposable methacrylate cuvettes (Cat: 9014, Perfector Scientific, Atascadero, CA) with an optical path length of 1 cm. Cuvettes were placed in a portable UV−vis spectrometer (USB2000+XR1-ES Ocean Optics, Dundin, FL) and mixed with a micro magnetic stirring bar, driven by an external magnetic mixer (Cat: H370170000, Scienceware, Wayne, NJ).

The colorimetric detection assay consists of final concentrations of 40 μM MB (CAS: 7220−79−3, Sigma−Aldrich, St. Louis, MO), 10 mM Sodium Borohydride (CAS: 16940−66−2, Sigma−Aldrich, St. Louis, MO), and 10 mM N-(2-hydroxyethyl) piperazine-N′-(2-ethanesulfonic acid) (HEPES, CAS: 7365−45−9 Sigma−Aldrich, St. Louis, MO) at pH 7. We chose HEPES as a buffering agent to maintain the pH constant during our experimental procedures and to minimize dye oxidation, which is a common reaction mechanism when reduced MB is in the presence of oxygen.[42,43] The 10 mM buffer concentration has sufficient buffering capacity without inducing particle instability, that is, aggregation due to reduction in electric double layer thickness or surface charge as a result of high ionic strength. All aqueous solutions were prepared by using ultra purified water (18.3 MΩ-cm, Milli-Q Advantage A10 system, Millipore Corp., Billerica, MA) and passed through a 200 nm, sterile filter (CAS: 28145−477, VWR international, Radnor, PA). We did not use any surfactants, dispersion stabilizing chemicals, or filtration processes in our complex matrices to avoid the perturbation of the particles or the complex media.

Nanoparticles as a Redox Catalyst and Colorimetric Quantification. We investigated the catalytic activity of NPs in the presence of MB and sodium borohydride (BH_4). We prepared our working suspension by dispersing nanoparticles in ultrapure water, environmental or biological medium. The resulting suspension was placed on a rotary shaker (50 rpm) for 1 h at room temperature (23 °C) prior to each experiment. We begin each experiment by mixing for ∼2 min our ENPs working suspension with a small aliquot of concentrated BH_4 and HEPES solution to reach a final concentration of 10 mM for both reagents. Then, we add a small volume of concentrated dye that provides a final concentration of 40 μM in a 2.5 mL working volume. We continuously monitor the absorbance of our colorimetric assay at the maximum dye's absorbance peak of λ_{max} = 665 nm. The concentration of particles reported is the mass of particles per mass of the original sample matrix (e.g., water, lake water, urine, etc.) before any necessary dilutions.

Figure 1B shows the UV−vis absorbance spectra of MB-BH_4 solution in the presence of NPs as a function of wavelength. The absorbance of methylene blue and sodium borohydride exhibit a maximum peak (λ_{max}) at 665 nm that corresponds to the n-π* bond transition associated with the presence of a C═S^+ chromophore group.[44] When 5 nm gold nanoparticles coated with tannic acid (Au_{TA}) are added to solution at the final concentration of 1 ppm, the absorbance decreases with time as MB is reduced to leukomethylene blue (LMB) through a nanoparticle catalytic electron transfer process.[45,46] We detect the catalytic activity of NPs by monitoring the optical density (OD) at 665 nm.

Figure 2 shows OD of dye-reductant solution at 665 nm as a function of time. MB-BH_4 solution in the absence of NPs has a stable OD of ∼2.8 for ∼25 s. The stable background indicates that the dye reduction is insignificant when nanoparticles are not in solution. We measured the optical density of dye-reductant for long experimental times, ∼1 h, in absence of NPs for ultra pure water and in complex matrices, and show that OD decreases less than 0.09 over the duration of the experiment (data presented in SI Figure S2). After 25 s, 100 nm Au_{TA} are added to the solution with a final concentration of 300 ppb which results in an exponential decrease of OD from 2.8 to 2.2 over ∼75 s. Then, the OD plateaus and remains steady for the duration of the experiment. We fit the absorbance as a function of time with an exponential curve, given as,

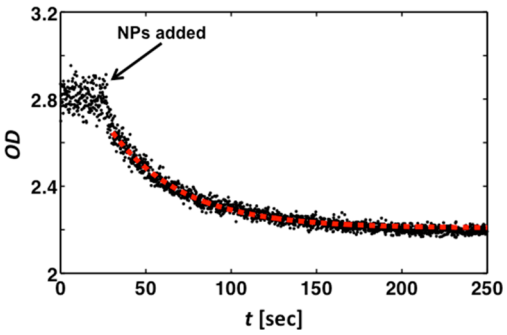

Figure 2. Optical density of Methylene Blue at pH 7.0 (10 mM $NaBH_4$ and 10 mM HEPES) in the presence of 100 nm gold nanoparticles coated with tannic acid (Au_{TA}) at a fixed mass concentration of 300 ppb recorded at 665 nm. Dash line indicates a fit to an exponential decay model. β is the asymptotic value of the optical density. Nanoparticles are added at t = 28 s causing MB−BH_4 optical density to decrease due to reduction of MB.

$$OD = OD_0 \exp(-(t/\tau)) + \beta \quad (1)$$

where the OD is the optical density of solution, OD_0 is the optical density at t = 0, τ is the exponential decay rate constant, t is the time transpired from the addition of the NP, and β is a constant that represents the asymptotic OD value. We fit τ and β values (41.8 s and 2.2 for the data shown in Figure 2), which respectively represent the decay time at which the dye absorbance is reduced to 1/e of its initial value and the steady state OD that is reached at long times. We determine the limit of detection (LOD) and limit of quantification (LOQ) for this assay in ultrapure water and in complex matrices. LOD and LOQ definitions and mathematical formulation details can be

DOI: 10.1021/es504350j
Environ. Sci. Technol. 2015, 49, 3611−3618

found in SI. β, LOD, and LOQ values allowed us to quantitatively compare concentrations, sizes, surface coatings, and core compositions of NPs in a variety of matrices.

RESULTS AND DISCUSSION

Role of Nanoparticle Concentration, Size, and Surface Area. The reduction of MB by borohydride depends directly on the concentration of nanoparticles. Figure 3 shows the dependence of the measured β values on the NPs mass concentration for 5 nm Au_{TA}. All β values are reported herein as the mean of at least four experimental measurements with error bars that denote the 95% confident intervals (α = 0.05). In the absence of nanoparticles in the MB-BH_4 solution, the β value is ~2.8, representing the highest absorbance of dye solution. β values decrease as NPs' mass concentration (mass of particle per volume) increases. Mass concentration should directly correlate with the reduction of the dye's absorbance since the number of metal particles, and their surface area, available to serve as an electron relay between MB and BH_4 increases as particle concentration increases. At 325 ppb or higher concentrations of Au_{TA} the β approaches zero suggesting a complete reduction of the MB. The limit of detection (LOD) of 5 nm Au_{TA} in buffered water is 89 ppb with a 95% confidence level.

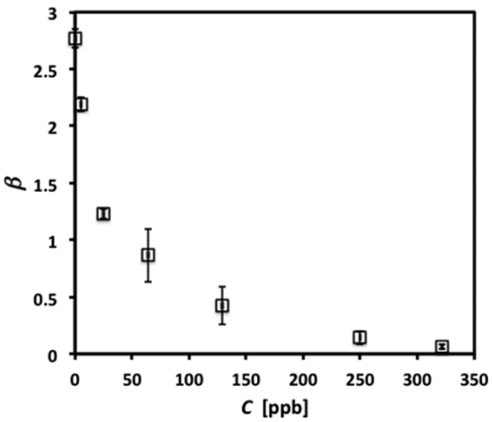

Figure 3. β-values as a function of gold nanoparticle concentration, C, coated with tannic acid (Au_{TA}) at a diameter of 5 nm. Each experimental value represents the mean value from a set of four experiments with error bars that correspond to 95% confidence intervals.

We studied the dependence of dye absorbance on NP size and surface area. Figure 4A shows β values as a function of particle size for Au_{TA} for three different constant surface areas 0.1, 0.2, and 0.5 cm^2. The average β values decrease with increasing surface area because higher surface area provides more surface sites for the electron transfer from reducing agent to the dye.[47−50] For constant surface area, β increases rapidly as particle size increases until it reaches 20 nm and then remains nearly constant for larger diameters. Previous studies have shown that the redox potential of particles decrease as a function of radius which would result in an increase the electron relay of the MB-BH_4 and lower effective β values.[26,27,50,51]

Figure 4B shows β as a function of nanoparticle surface area for 10, 20, 50, and 100 nm Au_{TA}. By increasing NP surface area, β values decrease linearly. We expect this linear trend because redox reaction rates (e.g., MB to LMB), can be predicted by the Butler−Volmer equation in the Tafel regime, expressed as,[52]

$$J = \frac{Ai_0}{zF}\exp((anF/RT)(E - E_0)) \tag{2}$$

where A is the total surface area of all NPs in the system, z is the valence electrons of the reacting species, α is the charge transfer coefficient, n is the number of electrons in the charge transfer process, i_0 is the exchange current density that is specific for the reaction (dye-NP pair), E is the electrical potential of NPs, and E_0 is the equilibrium potential for the redox reaction. This equation indicates that reaction rate depends linearly on the surface area, A, and implicitly on particle composition, through i_0 and E_0.[29] i_0 and E_0 are constant for a specific redox reaction and are determined by the dye and NP used in the system. The equilibrium potential depends on the difference between the reduction potential of the nanoparticle and the dye. Since MB has a constant reduction potential at constant pH, the rate is determined by the reduction potential of the NP. For each particle and redox chemistry, i_0 and E_0 are constant. From this equation, we gain an intuition about how the particle concentration, size, and composition impact the reaction rate.

Role of Capping Agents and NPs Core Composition. NPs are frequently functionalized with a variety of materials such as synthetic polymers, biopolymers, dendrimers, or other small molecules to provide stability, biocompatibility, and

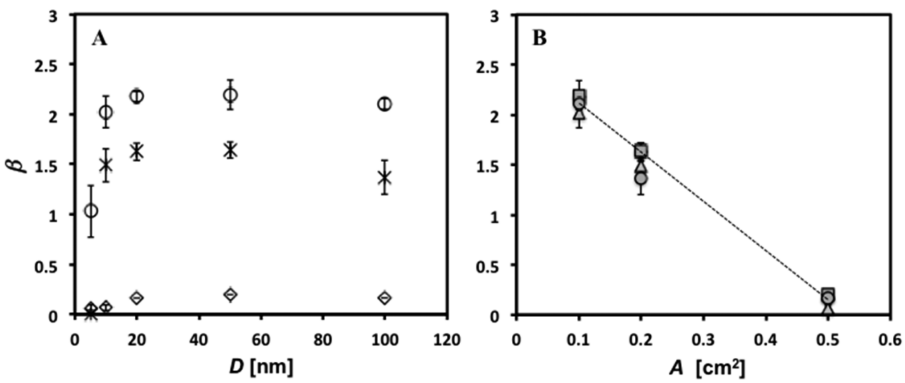

Figure 4. (A) Plot of β values as a function of Au_{TA} diameter at a surface area of 0.5 (◇), 0.2 (×), and 0.1 cm^2 (○) at fix NP mass concentration. (B) Plot of β values as a function of Au_{TA} surface area at 10 (triangles), 20 (diamonds), 50 (squares), and 100 nm (circles) particle diameters. All values represent the mean value of four experiments with error bars that correspond to 95% confidence intervals.

DOI: 10.1021/es504350j
Environ. Sci. Technol. 2015, 49, 3611−3618

functionality. In addition, these functional groups may facilitate or impede the electron transfer mechanism at the nanoparticle's surface. Figure 5 shows β values for 20 nm Au nanoparticles as

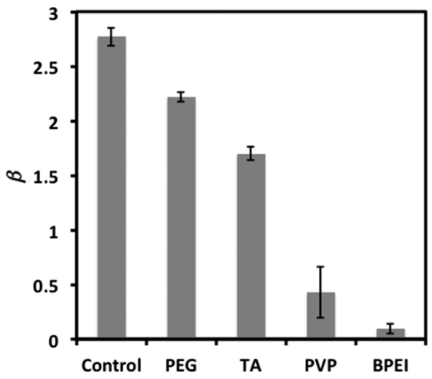

Figure 5. β-values as a function of NPs capping agent at a fix NP diameter of 20 nm and 500 ppb mass concentration of gold nanoparticles. Control experiments correlate to absence of NPs in the assay. β-values are an average over four experiments with error bars that denote 95% confidence intervals.

a function of capping agents at a constant particle concentration of 500 ppb. The β values range from 2.25 for Au_{PEG} to 0.18 for Au_{BPEI}. Lower β values correspond to higher NPs catalytic activity. At fixed NP diameter and core composition, the surface charge of nanoparticles has a high influence on the catalytic reactivity of NPs. Positively charged NPs possess higher reactivity than negatively charged particles. We believe positively charged particles (Au_{BPEI}), with a surface charge of +29.6 ± 17.6 mV, may electrostatically attract BH_4 molecules to the surface of the particle, which then enhances the reduction of MB, resulting in low β values. In contrast, we observe less dye reduction (high β values) on negatively charged particle surfaces, such as that for PVP and TA (−33.5 ± 18.9 and −16.3 ± 8.9 mV, respectively). The inhibition of MB reduction when NPs have a negatively charged surface coating might be explained by an electrostatic repulsion between functional groups and BH_4 molecules. According to Jiang et al. and Azad et al., when BH_4 absorbs to the surface of NPs, it creates a negatively charged layer that attracts cationic organic dyes, such as MB. This electrostatic attraction between the cationic dye and the reducing agents increase the reduction rate of MB.[53,54] To further understand the effect of dye reduction due to the effect of particles' capping agents, we also consider the molecular weight of the synthetic polymers. Figure 5 shows that β values decrease as molecular weight increases for the NPs' capping agents. BPEI, PVP, and PEG have molecular weights of 25, 10, and 5 kDa, respectively. Since the electron transfer between MB and BH_4 occurs at the surface of NP, we hypothesize that low molecular weight polymers will inhibit the reduction process of MB (high β values) by creating a steric repulsion between the dye and reducing agent at the particle surface. This repulsion is likely due to low molecular weight coatings having a larger fractional polymeric coverage on nanoparticles, creating a barrier to large molecules, such as MB, to NPs surfaces.[55] Taking together particle surface charge and molecular weight, β values are likely to decrease (more reactive) when particle surface charge has net positive value and when molecular weight of the capping agent increases. Recent studies suggest that the hydrophobicity of the dye, complex formation of the dye with anionic surfactants, repulsion between the dye and charged surfactants, may also impact the catalytic reactivity of the NPs.[54,56,57] The study of these factors is ongoing work in our lab.

We examine the surface catalytic reactivity of NPs over a range of particle compositions. The quantitative comparison of the catalytic activity of different nanoparticles is challenging since the reduction of MB in our assay is proportional to NP size, core composition, surface coatings, etc. Here, we provide a single-value to compare different NP core compositions and sizes that can potentially be used as a screen tool for detection of the presence/absence in systems with multiple nanoparticles types. $C_\beta = 2$ is the concentration of NPs (ppm) needed to decrease the OD of the solution to 2 (i.e., β value of 2). An OD of 2 represents a change in absorbance greater than 10 standard deviations of the background experiments. Figure 6 shows $C_\beta =$

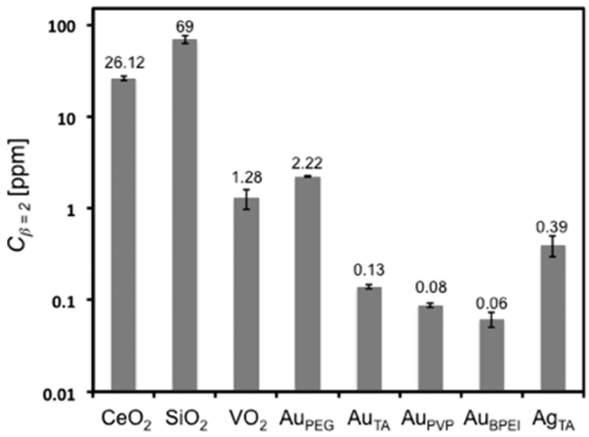

Figure 6. NPs concentration needed to reach a β value of 2 as a function of particle core composition and surface coating. Concentration values were extracted from a set of four experiments and shown as a mean value, with exact value shown above each bar, with error bars that represent 95% confidence intervals.

2 for commercially available particles with various core compositions, particle diameters, and surface coatings. $C_\beta = 2$ for metal nanoparticles (e.g., Au and Ag) ranges from 80 ppb to 4 ppm depending on core composition and particle surface functionally. Similarly, we are able to detect oxide nanoparticles (e.g., CeO_2, SiO_2, VO_2) in the range of 2 ppm to 69 ppm. The data suggests that the concentration needed to reduce dye-reductant solution is lower for elemental metal NPs than oxides nanoparticles, which indicates that Au and Ag NPs have a higher catalytic activity than oxide ones. The electron transfer, BH_4 to MB, may have a higher rate for metal NPs since this set of nanoparticles has higher electron conductivity than metal oxides. Our results suggest CeO_2 and SiO_2 can transfer electrons from BH_4 to MB similar to TiO_2 (5 nm) and ZnO (6 nm) which have been shown to transfer electrons to organic radicals, like MB.[58] Despite the differences in the core composition, particle diameter, and surface functionality, MB-BH_4 assay is able to assess the catalytic activity of NPs in concentrations (80 ppb to 69 ppm) typically used in environmental exposures models and measurements for nanomaterials hazard studies.[59] While we expect that oxide particles to show lower catalytic activity than metallic ones, more data is needed to explicitly detail the role of the composition and surface coatings. Our work represents a step toward the development of sensitive and reliable methodology to detect a variety of NPs.

DOI: 10.1021/es504350j
Environ. Sci. Technol. 2015, 49, 3611−3618

Detection of NPs in Biological and Environmental Matrices. Most analytical methods used for detecting and quantifying NPs in complex samples require careful sample preparation such as extraction, digestion, or sample fixation. Here we examine the sensitivity and efficacy of our colorimetric detection assay by determining LOD and LOQ values in complex environmental and biological media. We performed a series of calibration experiments for each of the complex matrices in order to extract LOD and LOQ values, as presented in SI. In the case of urine and serum, samples were diluted 4 and 5 times, respectively, to obtain a detectable signal. We report the concentration of the original suspension. In Table 1, we present LOD and LOQ values for 20 nm Au_{TA} in ultra pure water, environmental (e.g., lake water, NOM) and biological matrices (e.g., artificial urine, mouse serum). For the case of gold nanoparticles, the LOD ranges from 0.15 to 1.75 ppm depending on the matrix. The highest LOD values were observed for urine and serum at 1.75 and 1.53 ppm, respectively. Similarly, we have tested high nanoparticle concentrations, >60 ppm, that provided a complete reduction of the dye indicating that higher concentrations of NPs will lead to a β value of zero. Urine has an ionic strength of ~170 mM and conductivity of 6.6 mS cm^{-1}, which may reduce the catalytic activity of NPs by inducing particle aggregation. In the case of serum, the absorption of proteins and other biomolecules to the surface of the particles may inhibit the catalytic activity of NPs by creating proteins coronas that will obstruct the area where dye reduction take place.[60,61] For NOM and lake water, the LOD values were 1 order of magnitude lower than serum and urine. These data suggest that the catalytic assay proposed here to detect NPs in biological and environmental matrices as well as ultrapure water is simple and does not require complex instrumentation.

Table 1. Detection Limit Values for 20 nm Gold Nanoparticles Coated with Tannic Acid in Complex Matrices

matrix	LOD [ppm]	LOQ [ppm]
lake water	0.157	0.526
ultra pure water	0.303	1.012
NOM	0.460	1.536
blood serum	1.536	5.131
urine	1.759	5.864

We have developed a simple and affordable methodology to screen for the presence of NPs in complex samples (environmental waters and biological fluids). In this paper, we present a catalytic-colorimetric method for screening a wide range of NPs in complex matrices which may aid in the detection of nanoparticles for environmental, industrial, and medical applications. The method is sufficiently sensitive to surface reactivity—which is a unique nanoscale property of environmental relevance in NP toxicity, and uses inexpensive, commercially available reagents. This assay has detection limits below the typical concentrations commonly used in toxicological studies[5,62] with an analytical sensitivity in the range reported for LC_{50} concentration values.[63,64] Our results demonstrate that this assay can detect the presence of some NPs at ppb concentration levels. We have detected a wide range of metal (e.g., Ag and Au) and metal oxide (e.g., CeO_2, SiO_2, VO_2) NPs with a diameter range of 5−400 nm and multiple capping agents. The detection capabilities of this assay enable the assessment of NPs in serum, urine, environmental waters, and natural organic matter without any sample preparation or complex instrumentation. Incidental or endogenous nanoparticles may pose a challenge for the colorimetric assay. As a first step, we showed that this assay is not susceptible to false positive readings in lake water, which most likely contains endogenous nanoparticles, however we can not draw general conclusions about the assay's efficacy in the presence of all incidental and natural nanoparticles. Future work will focus on the assessment of background nanoparticles, the development of dye-reducing agent pairs that will be specific for a NPs' physicochemical characteristics (e.g., composition, size, concentration, redox potential, reactivity), as well as testing commercial nanoenabled products during their life cycle. We are also interested in correlating the NP's catalytic activity measured using this assay with the formation of reactive oxygen species (ROS) in cellular toxicity assays.[65−67] Our work represents a step toward reliable, sensitive, and accurate methodologies for the detection of NPs in complex matrices, using low-cost and portable instrumentation.

■ ASSOCIATED CONTENT

Supporting Information

Serum collection, VO_2 Synthesis and characterization, ICPMS analysis, dynamic light scattering characterization of NPs, control analysis of colorimetric assay, limit of detection and limit of quantification are available as Supporting Information. This material is available free of charge via the Internet at http://pubs.acs.org.

■ AUTHOR INFORMATION

Corresponding Author

*Phone: +1 (206) 543-9834; fax: +1 (206) 685-8047; e-mail: jposner@uw.edu.

Notes

The authors declare no competing financial interest.

■ ACKNOWLEDGMENTS

This material is based upon work supported by the National Science Foundation Graduate Research Fellowship for C. Corredor under grants DGE-0718124 and DEG-1256082, as well as NIH Grand Opportunities (RC2) program through NANO-GO NIEHS grant DE-FG02-08ER64613, NSF (CBET-1160772), and EPA (RD83558001). We thank Evan Uchaker at the University of Washington (UW) for providing VO_2 NPs, Megan M. Cartwright and Prof. Terrance J. Kavanagh at the UW Nanotoxicology Center for collecting the mouse serum, Prof. Kyle Doudrick at the University of Notre Dame for valuable discussions, Yu Yang at Arizona State University for ICPMS measurements, and William Walker at the UW Bioengineering department for preparing the table of content (TOC) graphic.

■ REFERENCES

(1) Borm, P. J. A.; Kreyling, W. Toxicological hazards of inhaled nanoparticles—Potential implications for drug delivery. *J. Nanosci. Nanotechnol.* **2004**, *4*, 521−531.

(2) Nel, A.; Xia, T.; Mädler, L.; Li, N. Toxic potential of materials at the nanolevel. *Science* **2006**, *311*, 622−627.

(3) De Jong, W. H.; Borm, P. J. Drug delivery and nanoparticles: Applications and hazards. *Int. J. Nanomedicine* **2008**, *3*, 133−149.

(4) Edson, J. A.; Kwon, Y. J. RNAi for silencing drug resistance in microbes toward development of nanoantibiotics. *J. Controlled Release.*

DOI: 10.1021/es504350j
Environ. Sci. Technol. 2015, 49, 3611−3618

(5) Weir, A.; Westerhoff, P.; Fabricius, L.; Hristovski, K.; von Goetz, N. Titanium dioxide nanoparticles in food and personal care products. *Environ. Sci. Technol.* **2012**, *46*, 2242−2250.
(6) Scheufele, D. A.; Corley, E. A.; Dunwoody, S.; Shih, T.-J.; Hillback, E.; Guston, D. H. Scientists worry about some risks more than the public. *Nat. Nanotechnol.* **2007**, *2*, 732−734.
(7) Corredor, C.; Hou, W.-C.; Klein, S. A.; Moghadam, B. Y.; Goryll, M.; Doudrick, K.; Westerhoff, P.; Posner, J. D. Disruption of model cell membranes by carbon nanotubes. *Carbon* **2013**, *60*, 67−75.
(8) Hendren, C. O.; Mesnard, X.; Dröge, J.; Wiesner, M. R. Estimating production data for five engineered nanomaterials as a basis for exposure assessment. *Environ. Sci. Technol.* **2011**, *45*, 2562−2569.
(9) Lesniak, A.; Salvati, A.; Santos-Martinez, M. J.; Radomski, M. W.; Dawson, K. A.; Åberg, C. Nanoparticle adhesion to the cell membrane and its effect on nanoparticle uptake efficiency. *J. Am. Chem. Soc.* **2013**, *135*, 1438−1444.
(10) Varela, J. A.; Bexiga, M. G.; Åberg, C.; Simpson, J. C.; Dawson, K. A. Quantifying size-dependent interactions between fluorescently labeled polystyrene nanoparticles and mammalian cells. *J. Nanobiotechnol.* **2012**, *10*, 39.
(11) Koch, A. M.; Reynolds, F.; Merkle, H. P.; Weissleder, R.; Josephson, L. Transport of surface-modified nanoparticles through cell monolayers. *Chembiochem* **2005**, *6*, 337−345.
(12) Chen, M.; von Mikecz, A. Formation of nucleoplasmic protein aggregates impairs nuclear function in response to SiO_2 nanoparticles. *Exp. Cell Res.* **2005**, *305*, 51−62.
(13) Brunner, T. J.; Wick, P.; Manser, P.; Spohn, P.; Grass, R. N.; Limbach, L. K.; Bruinink, A.; Stark, W. J. In vitro cytotoxicity of oxide nanoparticles: Comparison to asbestos, silica, and the effect of particle solubility. *Environ. Sci. Technol.* **2006**, *40*, 4374−4381.
(14) Negoda, A.; Liu, Y.; Hou, W.-C.; Corredor, C.; Moghadam, B. Y.; Musolff, C.; Li, L.; Walker, W.; Westerhoff, P.; Mason, A. J.; et al. Engineered nanomaterial interactions with bilayer lipid membranes: Screening platforms to assess nanoparticle toxicity. *Int. J. Biomed. Nanosci. Nanotechnol.* **2013**, *3*, 52−83.
(15) Li, K.; Chen, Y.; Zhang, W.; Pu, Z.; Jiang, L.; Chen, Y. Surface interactions affect the toxicity of engineered metal oxide nanoparticles toward paramecium. *Chem. Res. Toxicol.* **2012**, *25*, 1675−1681.
(16) Gou, N.; Onnis-Hayden, A.; Gu, A. Z. Mechanistic toxicity assessment of nanomaterials by whole-cell-array stress genes expression analysis. *Environ. Sci. Technol.* **2010**, *44*, 5964−5970.
(17) Lowry, G. V.; Gregory, K. B.; Apte, S. C.; Lead, J. R. Transformations of nanomaterials in the environment. *Environ. Sci. Technol.* **2012**, *46*, 6893−6899.
(18) Levard, C.; Hotze, E. M.; Lowry, G. V.; Brown, G. E. Environmental transformations of silver nanoparticles: Impact on stability and toxicity. *Environ. Sci. Technol.* **2012**, *46*, 6900−6914.
(19) Zhang, Y.; Chen, Y.; Westerhoff, P.; Hristovski, K.; Crittenden, J. C. Stability of commercial metal oxide nanoparticles in water. *Water Res.* **2008**, *42*, 2204−2212.
(20) Benn, T. M.; Westerhoff, P. Nanoparticle silver released into water from commercially available sock fabrics. *Environ. Sci. Technol.* **2008**, *42*, 4133−4139.
(21) Doudrick, K.; Herckes, P.; Westerhoff, P. Detection of carbon nanotubes in environmental matrices using programmed thermal analysis. *Environ. Sci. Technol.* **2012**, *46*, 12246−12253.
(22) Plata, D. L.; Reddy, C. M.; Gschwend, P. M. Thermogravimetry−mass spectrometry for carbon nanotube detection in complex mixtures. *Environ. Sci. Technol.* **2012**, *46*, 12254−12261.
(23) Gao, C.; Weisman, D.; Gou, N.; Ilyin, V.; Gu, A. Z. Analyzing high dimensional toxicogenomic data using consensus clustering. *Environ. Sci. Technol.* **2012**, *46*, 8413−8421.
(24) Laoufi, I.; Saint-Lager, M.-C.; Lazzari, R.; Jupille, J.; Robach, O.; Garaudée, S.; Cabailh, G.; Dolle, P.; Cruguel, H.; Bailly, A. Size and catalytic activity of supported gold nanoparticles: An in operando study during CO oxidation. *J. Phys. Chem. C* **2011**, *115*, 4673−4679.
(25) Haruta, M.; Yamada, N.; Kobayashi, T.; Iijima, S. Gold catalysts prepared by coprecipitation for low-temperature oxidation of hydrogen and of carbon monoxide. *J. Catal.* **1989**, *115*, 301−309.
(26) Jana, N. R.; Wang, Z. L.; Pal, T. Redox catalytic properties of palladium nanoparticles: Surfactant and electron donor−acceptor effects. *Langmuir* **2000**, *16*, 2457−2463.
(27) Jana, N. R.; Pal, T. Redox catalytic property of still-growing and final palladium particles: A comparative study. *Langmuir* **1999**, *15*, 3458−3463.
(28) Nath, S.; Praharaj, S.; Panigrahi, S.; Basu, S.; Pal, T. Photochemical evolution of palladium nanoparticles in Triton X-100 and its application as catalyst for degradation of acridine orange. *Curr. Sci.* **2007**, *92*, 786−790.
(29) Plieth, W. J. Electrochemical properties of small clusters of metal atoms and their role in the surface enhanced Raman scattering. *J. Phys. Chem.* **1982**, *86*, 3166−3170.
(30) Mallick, K.; Witcomb, M.; Scurrell, M. Silver nanoparticle catalysed redox reaction: An electron relay effect. *Mater. Chem. Phys.* **2006**, *97*, 283−287.
(31) Cheval, N.; Gindy, N.; Flowkes, C.; Fahmi, A. Polyamide 66 microspheres metallised with in situ synthesised gold nanoparticles for a catalytic application. *Nanoscale Res. Lett.* **2012**, *7*, 182.
(32) Gillman, P. K. CNS toxicity involving methylene blue: The exemplar for understanding and predicting drug interactions that precipitate serotonin toxicity. *J. Psychopharmacol.* **2011**, *25*, 429−436.
(33) Krishnan, M.; Nalaskowski, J. W.; Cook, L. M. Chemical mechanical planarization: Slurry chemistry, materials, and mechanisms. *Chem. Rev.* **2009**, *110*, 178−204.
(34) Uchaker, E.; Zheng, Y. Z.; Li, S.; Candelaria, S. L.; Hu, S.; Cao, G. Z. Better than crystalline: Amorphous vanadium oxide for sodium-ion batteries. *J. Mater. Chem. A* **2014**, *2*, 18208−18214.
(35) Haber, J. Fifty years of my romance with vanadium oxide catalysts. *Catal. Today* **2009**, *142*, 100−113.
(36) Jarrell, J. D.; Dolly, B.; Morgan, J. R. Rapid screening, in vitro study of metal oxide and polymer hybrids as delivery coatings for improved soft-tissue integration of implants. *J. Biomed. Mater. Res., Part A* **2010**, *92*, 1094−1104.
(37) Benn, T.; Cavanagh, B.; Hristovski, K.; Posner, J. D.; Westerhoff, P. The release of nanosilver from consumer products used in the home. *J. Environ. Qual.* **2010**, *39*, 1875.
(38) Benn, T. M.; Westerhoff, P. Nanoparticle silver released into water from commercially available sock fabrics. *Environ. Sci. Technol.* **2008**, *42*, 4133−4139.
(39) Thapa, P. B.; Nakajima, F.; Furumai, H. Characterization of natural organic matter in a shallow eutrophic lake. *Water Sci. Technol.* **2002**, *46*, 465−471.
(40) Wenzler-Röttele, S.; Dettenkofer, M.; Schmidt-Eisenlohr, E.; Gregersen, A.; Schulte-Mönting, J.; Tvede, M. Comparison in a laboratory model between the performance of a urinary closed system bag with double non-return valve and that of a single valve system. *Infection* **2006**, *34*, 214−218.
(41) Uchaker, E.; Gu, M.; Zhou, N.; Li, Y.; Wang, C.; Cao, G. Enhanced intercalation dynamics and stability of engineered micro/nano-structured electrode materials: Vanadium oxide mesocrystals. *Small* **2013**, *9*, 3880−3886.
(42) Galagan, Y.; Su, W.-F. Reversible photoreduction of methylene blue in acrylate media containing benzyl dimethyl ketal. *J. Photochem. Photobiol. Chem.* **2008**, *195*, 378−383.
(43) Impert, O.; Katafias, A.; Kita, P.; Mills, A.; Pietkiewicz-Graczyk, A.; Wrzeszcz, G. Kinetics and mechanism of a fast leuco-Methylene Blue oxidation by copper(II)−halide species in acidic aqueous media. *Dalton Trans.* **2003**, 348−353.
(44) Heger, D.; Jirkovsky, J.; Klan, P. Aggregation of Methylene Blue in frozen aqueous solutions studied by absorption spectroscopy. *J. Phys. Chem. A* **2005**, *109*, 6702−6709.
(45) Spiro, M.; Freund, P. L. Colloidal catalysis. Transport versus surface control. *J. Chem. Soc. Faraday Trans. 1* **1983**, *79*, 1649−1658.
(46) Spiro, M. Heterogeneous catalysis in solution. Part 17.—Kinetics of oxidation−reduction reaction catalysed by electron transfer through the solid: An electrochemical treatment. *J. Chem. Soc. Faraday Trans. 1* **1979**, *75*, 1507−1512.

DOI: 10.1021/es504350j
Environ. Sci. Technol. 2015, 49, 3611−3618

(47) Belloni, J. Metal nanocolloids. *Curr. Opin. Colloid Interface Sci.* **1996**, *1*, 184−196.
(48) Henglein, A. Small-particle research: Physicochemical properties of extremely small colloidal metal and semiconductor particles. *Chem. Rev.* **1989**, *89*, 1861−1873.
(49) Henglein, A. Physicochemical properties of small metal particles in solution: "Microelectrode" reactions, chemisorption, composite metal particles, and the atom-to-metal transition. *J. Phys. Chem.* **1993**, *97*, 5457−5471.
(50) Jana, N. R.; Sau, T. K.; Pal, T. Growing small silver particle as redox catalyst. *J. Phys. Chem. B* **1999**, *103*, 115−121.
(51) Chang, Y.-C.; Chen, D.-H. Catalytic reduction of 4-nitrophenol by magnetically recoverable Au nanocatalyst. *J. Hazard. Mater.* **2009**, *165*, 664−669.
(52) Tang, L.; Li, X.; Cammarata, R. C.; Friesen, C.; Sieradzki, K. Electrochemical stability of elemental metal nanoparticles. *J. Am. Chem. Soc.* **2010**, *132*, 11722−11726.
(53) Jiang, Z.-J.; Liu, C.-Y.; Sun, L.-W. Catalytic properties of silver nanoparticles supported on silica spheres. *J. Phys. Chem. B* **2005**, *109*, 1730−1735.
(54) Azad, U. P.; Ganesan, V.; Pal, M. Catalytic reduction of organic dyes at gold nanoparticles impregnated silica materials: Influence of functional groups and surfactants. *J. Nanoparticle Res.* **2011**, *13*, 3951−3959.
(55) Berg, J. C. *An Introduction to Interfaces and Colloids: The Bridge to Nanoscience*; World Scientific: Singapore; Hackensack, NJ, 2009.
(56) Bergmann, K.; O'Konski, C. T. A spectroscopic study of methylene blue monomer, dimer, and complexes with montmorillonite. *J. Phys. Chem.* **1963**, *67*, 2169−2177.
(57) Pande, S.; Ghosh, S. K.; Nath, S.; Praharaj, S.; Jana, S.; Panigrahi, S.; Basu, S.; Pal, T. Reduction of methylene blue by thiocyanate: Kinetic and thermodynamic aspects. *J. Colloid Interface Sci.* **2006**, *299*, 421−427.
(58) Schrauben, J. N.; Hayoun, R.; Valdez, C. N.; Braten, M.; Fridley, L.; Mayer, J. M. Titanium and zinc oxide nanoparticles are proton-coupled electron transfer agents. *Science* **2012**, *336*, 1298−1301.
(59) Holden, P. A.; Klaessig, F.; Turco, R. F.; Priester, J. H.; Rico, C. M.; Avila-Arias, H.; Mortimer, M.; Pacpaco, K.; Gardea-Torresdey, J. L. Evaluation of exposure concentrations used in assessing manufactured nanomaterial environmental hazards: Are they relevant? *Environ. Sci. Technol.* **2014**, *48*, 10541−10551.
(60) Lundqvist, M.; Stigler, J.; Elia, G.; Lynch, I.; Cedervall, T.; Dawson, K. A. Nanoparticle size and surface properties determine the protein corona with possible implications for biological impacts. *Proc. Natl. Acad. Sci. U. S. A.* **2008**, *105*, 14265−14270.
(61) Lesniak, A.; Fenaroli, F.; Monopoli, M. P.; Åberg, C.; Dawson, K. A.; Salvati, A. Effects of the presence or absence of a protein corona on silica nanoparticle uptake and impact on cells. *ACS Nano* **2012**, *6*, 5845−5857.
(62) Adams, L. K.; Lyon, D. Y.; Alvarez, P. J. J. Comparative eco-toxicity of nanoscale TiO_2, SiO_2, and ZnO water suspensions. *Water Res.* **2006**, *40*, 3527−3532.
(63) Sarkar, B.; Netam, S. P.; Mahanty, A.; Saha, A.; Bosu, R.; Krishnani, K. K. Toxicity evaluation of chemically and plant derived silver nanoparticles on zebrafish (*Danio rerio*). *Proc. Natl. Acad. Sci., India, Sect. B* **2014**, 1−8.
(64) Kovriznych, J. A.; Sotnikova, R.; Zeljenkova, D.; Rollerova, E.; Szabova, E.; Wimmerova, S. Acute toxicity of 31 different nanoparticles to zebrafish (*Danio rerio*) tested in adulthood and in early life stages - comparative study. *Interdiscip. Toxicol.* **2013**, *6*, 67−73.
(65) Li, Y.; Zhang, W.; Niu, J.; Chen, Y. Mechanism of photogenerated reactive oxygen species and correlation with the antibacterial properties of engineered metal-oxide nanoparticles. *ACS Nano* **2012**, *6*, 5164−5173.
(66) Zhang, W.; Li, Y.; Niu, J.; Chen, Y. Photogeneration of reactive oxygen species on uncoated silver, gold, nickel, and silicon nanoparticles and their antibacterial effects. *Langmuir* **2013**, *29*, 4647−4651.
(67) Zhang, H.; Ji, Z.; Xia, T.; Meng, H.; Low-Kam, C.; Liu, R.; Pokhrel, S.; Lin, S.; Wang, X.; Liao, Y.-P.; et al. Use of metal oxide nanoparticle band gap to develop a predictive paradigm for oxidative stress and acute pulmonary inflammation. *ACS Nano* **2012**, *6*, 4349−4368.

DOI: 10.1021/es504350j
Environ. Sci. Technol. 2015, 49, 3611−3618